LABEL-FREE AND REAGENTLESS ELECTROCHEMICAL GENOSENSOR BASED ON GRAPHENE ACID FOR MEAT ADULTERATION DETECTION

José M. R. Flauzino[1,2], Emily P. Nguyen[2], Qiuyue Yang[2], Giulio Rosati[2], David Panáček[2,3,4], Ana G. Brito-Madurro[1], João M. Madurro[1,5], Aristeidis Bakandritsos[3,6], Michal Otyepka[3,7], Arben Merkoçi[2*]

[1] Institute of Biotechnology, Federal University of Uberlândia, 38405-319, Uberlândia-MG, Brazil.

[2] Catalan Institute of Nanoscience and Nanotechnology, Autonomous University of Barcelona, 08193, Bellaterra, Barcelona, Spain.

[3] Regional Centre of Advanced Technologies and Materials, Czech Advanced Technology and Research Institute (CATRIN), Šlechtitelů 241/27, 783 71, Olomouc, Palacký University Olomouc, Czech Republic.

[4] Department of Physical Chemistry, Faculty of Science, Palacký University Olomouc, 17. listopadu 1192/12, 771 46 Olomouc, Czech Republic.

[5] Institute of Chemistry, Federal University of Uberlândia, 38400-902, Uberlândia-MG, Brazil.

[6] Nanotechnology Centre, Centre of Energy and Environmental Technologies, VŠB–Technical University of Ostrava, 17. listopadu 2172/15, 708 00 Ostrava-Poruba, Czech Republic.

[7] IT4Innovations, VŠB–Technical University of Ostrava, 17. listopadu 2172/15, 708 00 Ostrava-Poruba, Czech Republic.

*Corresponding author. Nanobioelectronics & Biosensors Group, Institut Català de Nanociància i Nanotecnologia (ICN2), CSIC and The Barcelona Institute of Science and Technology (BIST), Campus UAB, 08193, Bellaterra, Barcelona, Spain. E-mail address: arben.merkoci@icn2.cat

Abstract

With the increased demand for beef in emerging markets, the development of quality-control diagnostics that are fast, cheap and easy to handle is essential. Especially where beef must be free from pork residues, due to religious, cultural or allergic reasons, the availability of such diagnostic tools is crucial. In this work, we report a label-free impedimetric genosensor for the sensitive detection of pork residues in meat, by leveraging the biosensing capabilities of graphene acid - a densely and selectively functionalized graphene derivative. A single stranded DNA probe, specific for the pork mitochondrial genome, was immobilized onto carbon screen-printed electrodes modified with graphene acid. It was demonstrated that graphene acid improved the charge transport properties of the electrode, following a simple and rapid electrode modification and detection protocol. Using non-faradaic electrochemical impedance spectroscopy, which does not require any electrochemical indicators or redox pairs, the detection of pork residues in beef was achieved in a short-time of 45 min (including sample preparation), with a limit of detection of 9% w/w pork content in beef samples. Importantly, the sensor retained its performance properties unchanged for at least 4 weeks. These set of features places the present pork DNA sensor among the most attractive for further development and commercialization, as well lay the ground for the development of sensitive and selective sensing devices for label-free, fast, simple and reliable monitoring of meat purity.

Keywords: food adulteration; DNA biosensor; non-faradaic electrochemical impedance spectroscopy; beef; pork.

1 INTRODUCTION

The beef industry and the food demand are rapidly growing, mainly in developing countries, due to the rising population (Hansen, 2018). However, food adulteration in the meat industry is a recurring topic, where, in pieces of solid meat, adulteration is challenging, and processed meats, such as hamburgers and meatballs, the mixture of different types of meat is imperceptible (Rahmati et al., 2016). Final consumers, especially from groups with dietary restrictions (e. g. Halal and Kosher diet followers), must be sure of the origin of the meat they consume, especially regarding the total absence of pork, as well as there is a potential danger of serious allergic responses or intolerance to proteins derived from specific animals (Wilson and Platts-Mills, 2018).

Meat quality control analysis usually applies physical, sensory, anatomical and histological methods and, in rare cases, molecular techniques such as polymerase chain reaction (Okuma and Hellberg, 2015) and loop-mediated isothermal amplification (Kumar et al., 2017). However, these methods of beef purity analysis are time consuming, require special equipment, reagents and qualified personnel. Biosensors enter this scenario with the proposal to develop devices that are easy to handle, quick to respond, do not require qualified personnel and can be used in the various stages of the meat industry (Montiel et al., 2017; Singh et al., 2016).

Nucleic acid-based biosensors, also called genosensors (Ratajczak et al., 2018a, 2018b), are promising tools for meat adulteration analysis, because nucleic acids such DNA are more stable in meat processing steps than proteins (Hellberg et al., 2017). Meat, as a muscle tissue, contains cells including many mitochondria that hold mitochondrial DNA molecules. The mitochondrial DNA differs from the nuclear, because it is smaller, circular and present in larger quantity, making it a more promising target for detection techniques (Irwin et al., 1991). Within the different types of genosensors, those employing electrochemical techniques are fast-responding and easy to miniaturize, however, they in general require the use of DNA intercalants (De Castro et al., 2018), metal complexes (Moço et al., 2019) or other electroactive molecules (Flauzino et al., 2021a) including nanoparticles (De La Escosura-Muñiz et al., 2016; Merkoçi, 2010) for targeted detection,

which makes the sensing process more laborious, expensive and non-eco-friendly. Therefore, the search of new label-free and reagentless technologies is extremely important.

The definition of a label-free electrochemical biosensor is unclear in the literature. However, any molecule that is introduced into the medium, except for the electrolyte (generally a buffer or acid solution), the analyte and the immobilized biomolecule on the surface of the transducer, can be recognized as a label (Chen et al., 2019). Examples of employed labels in electrochemical biosensors are redox probes e. g. potassium ferro/ferricyanide (Oliveira et al., 2018a), electroactive mediators/intercalants such as methylene blue (Idili et al., 2021), ferrocene (Rabti et al., 2016) and ethidium bromide (Oliveira et al., 2018b) and enzymatic reaction indicators e. g. tetramethylbenzidine (Alves-Balvedi et al., 2016). Therefore, genuinely label-free electrochemical biosensors are rare, and their study is still open toward achieving better detection performance. Electrochemical impedance spectroscopy is a very sensitive technique and widely used in biosensors (Strong et al., 2021), and its non-faradaic version only requires a reagentless support electrolyte to perform the detection (Cecchetto et al., 2017; Rosati et al., 2019; Stevenson et al., 2018). The detection of small DNA fragments by hybridization in a label-free approach was proposed (Berggren et al., 1999), but it still remains a challenge in bioelectrochemistry. Nevertheless, new nanomaterials and platforms are making this type of detection more and more tangible.

The use of screen-printed carbon electrodes (SPCE) offers great advantages in bioelectrochemistry, since they are inexpensive and simple to build, though in general they need an additional matrix modification to be a suitable substrate for biomolecule immobilization (Thiyagarajan et al., 2014). Nanomaterials derived from carbon are excellent candidates for modifying SPCE, as they have an inherent affinity for the surface of the SPCE, can be conductive and may have functional groups that facilitate the immobilization of biomolecules (Quesada-González and Merkoçi, 2018; Ribeiro et al., 2020; Vermisoglou et al., 2020). Recently, new

fluorographene derivatives have been discovered (Chronopoulos et al., 2017), including graphene acid (Bakandritsos et al., 2017).

Graphene acid (GA) is a selectively, homogenously, and densely functionalized carboxylic graphene derivative. Its functionalization degree of 13 at% (corresponding to more than 30 mass% in carboxylic groups), its sheet resistance of 6800 Ω sq^{-1}, which is five orders of magnitude lower than that of graphene oxide, render GA the most conductive graphene derivative with such a high content in carboxyl groups. The titration profile of GA closely resembles that of molecular organic acids, with pK_a of 5.2, reflecting its well-defined structure. Such properties shape a great combination for bioelectrochemistry applications, allowing attachment of biomolecules on a conductive support (Seelajaroen et al., 2020). Its use was reported for chemical sensors, catalysis and supercapacitor applications (Blanco et al., 2019; Heng Cheong et al., 2019; Lenarda et al., 2019; Šedajová et al., 2020; Seelajaroen et al., 2020), but its potential application in biosensors has not yet been studied.

To this end, in this work we developed a new DNA biosensor for the detection of adulteration of beef with pork, utilizing as matrix graphene acid on SPCE via non-faradaic impedance spectroscopy, which is a label-free and reagentless electrochemical technique, measuring the admittance and capacitance of the biosensor surface after the DNA hybridization events.

2 MATERIAL AND METHODS

2.1 Chemicals and apparatus

All reagents were of analytical grade, without previous purification. Ultra-high purity water (18.2 MΩ cm^{-1}, Mili-Q, USA) was used for preparation of all solutions. Phosphate Saline Buffer solution (PBS, Sigma-Aldrich, USA, 10 mmol L^{-1}) was used as electrolyte and for DNA dilutions. $K_4[Fe(CN)_6]$, $K_3[Fe(CN)_6]$, Tris–HCl, EDTA, NaCl, H_2SO_4, Sodium dodecyl sulfate (SDS), 1-Ethyl-3-(3-dimethylaminopropyl)carbodiimide (EDC) and N-Hydroxysuccinimide (NHS) were purchased from Sigma-Aldrich, USA. Solutions utilized in electrochemical analyzes were

deoxygenated by ultrapure nitrogen bubbling in time proportional to volume (1 min mL^{-1}) before use.

All oligonucleotides were obtained from Biomers.net GmbH, Germany. The immobilized probe consisted on a single-stranded DNA oligonucleotide with the following sequence: 5'-(NH_2)AAAAAAAGCTGATAGTAGATTTGTGATGACCGTA-3'. This DNA probe has a 5' end amination for better attachment with the nanomaterial, a spacer consisting of a sequence of 7 adenines nucleotides and a 27 base sequence complementary with the pig (*Sus scrofa*) mitochondrial DNA, specifically with a region of the cytochrome b gene (Matsunaga et al., 1999). To perform hybridization detection tests, complementary (5'-TACGGTCATCACAAATCTACTATCAGC-3') and non-complementary (*Bos taurus* sequence: 5'-CTAGAAAAGTGTAAGACCCGTAATATA-3') were used.

All electrochemical measurements were conducted in an Autolab PGSTAT302N potentiostat (Netherlands) with a FRA2 module by NOVA 2.1.3. software, and data was analyzed and ploted utilizing Origin 2018 software. All data was presented as mean ± standard deviation, with an n = 3.

2.2 Meat sample preparation

Fig. 1 shows a scheme of the meat sample preparation. Knuckle beef and pork loin of low fat were purchased from a butchery in Barcelona, Catalunya, Spain.

<FIGURE 1>

The sample preparation was carried out according to literature with modifications (Khairil Mokhtar et al., 2020). 5.0 g of each meat samples where blend with 10 mL of ice-cold extraction buffer (0.2 mol L^{-1} Tris–HCl, 0.01 mol L^{-1} EDTA, 0.5 mol L^{-1} NaCl and 1% SDS v/v) with a hand blender for 5 minutes. After that, the samples were sonicated for 15 min at 80 ºC. This step is crucial to disrupt both cell and mitochondrial membranes, as well to facilitate DNA fragmentation.

Mitochondrial DNA is a large circular molecule of approximately 16.600 base pairs (bp), thus requiring smaller fragments to facilitate its interaction with the 27 bp DNA probe attached on the surface of the biosensor. The resulting solution was centrifuged (12.000 rpm, 15 min) and the upper phase was recovered. To minimize time and cost, no purification step was performed further. The DNA concentration in both beef and pork solutions were measured with a Nanodrop spectrophotometer (Thermo Fischer, USA), normalized with PBS solution to 100 ng mL^{-1} and stored at -20 ºC until use.

2.3 SPCE construction and modification with graphene acid

Lab-made SPCE were printed on heat-stabilized polyester films (Mac Dermide Enthone, USA) in a DEK 248 (UK) semi-automatic printer, utilizing commercial inks (Gwent Group/Sun Chemical, UK) by layer-by-layer strategy as follows: firstly C2180423D2 Silver Paste was printed to pattern the conductive paths and auxiliary electrodes, then C2130809D5 Silver/Silver Chloride Paste was printed for reference electrode, afterwards C2030519P4 Carbon Paste was printed for work (Ø = 3.1 mm) auxiliary electrodes. D2070423P5 Dielectric Paste was used for contact isolation and delimitation of the electrode areas. After each printing step, the substrate with printed materials was cured in the oven at 110 °C for 30 min. Prior to use, the SPCE were preconditioned by cyclic voltammetry in sulfuric acid solution (0.1 mol L^{-1}) between -0.5 and 1.2 V, 10 cycles, 100 mV s^{-1}, to ensure a surface free of impurities and to obtain a common voltammetric profile. Then, they were rinsed with deionized water and dried with N_2 gas. Graphene acid (GA) was synthetized as previous works (Bakandritsos et al., 2017). A GA suspension (1.00 mg mL^{-1}) was sonicated for 10 minutes then centrifuged (14.000 rpm, 10 min). The concentration of the suspension was mensurated before and after centrifugation with UV-vis spectroscopy (λ = 660 nm). The GA supernatant was drop-casted onto the working area of the SPCE (5 µL, dried at 37 ºC). The number of drop-casting rounds were optimized, with four consecutive rounds being tested, to ensure a

complete cover of the SPCE working area. Then, the SPCE was washed by immersion in PBS for 10 s and dried with N_2.

2.4 Genosensor construction

<FIGURE 2>

Fig. 2 shows a scheme of the electrode modification and the genosensor construction. In the modified SPCE working area, 10 µL of EDC/NHS solution (50 and 30 mmol L^{-1} respectively, freshly prepared in PBS) was added and kept in room temperature (25 ºC) for 1 hour, aiming the activation of the carboxyl groups of the GA and consequently attachment of the DNA probe. The electrodes were then washed by immersion in PBS for 10 s and dried with N_2. 10 µL of the DNA probe solution (10 µmol L^{-1}, PBS) was dropped onto the working area of the SPCE, and it was kept at 4 ºC for 12 h for the formation of the amide bonds between the nanomaterial and the 5' amino-terminal group of the DNA probe. Then, the electrodes were washed by immersion in PBS for 10 s and dried with N_2. To block possible active EDC/NHS sites, 10 µL of ethanolamine solution (1 mol L^{-1} in water) was added onto the working area of the SPCE and kept in room temperature for 10 minutes. Finally, the electrode was washed by immersion in PBS for 10 s and dried with N_2. This was the ready-to-use biosensor. To determine whether the immobilization process of the DNA probe was effective, Fourier-transform infrared spectroscopy (FTIR) analyzes were performed on the surface of the working electrode utilizing a PerkinElmer spectrophotometer in ATR (Attenuated Total Reflectance) mode, with and without the use of the EDC/NHS protocol, to verify the formation of the amide bonds.

2.5 Electrochemical characterization of the electrodes

Bare SPCE, SPCE modified with GA and the ready-to-use biosensor were characterized by cyclic voltammetry (CV) and electrochemical impedance spectroscopy (EIS) employing the well-known ferrocyanide/ferricyanide redox pair ($K_4[Fe(CN)_6]$ and $K_3[Fe(CN)_6]$, 1 mmol L^{-1}, in PBS solution 10 mmol L^{-1}). For the CV measurements 5 potential cycles from -0.5 to 0.8 V, 50 mV s^{-1} were applied, in which the anodic peak current (I_{pa}) and potential (E_{pa}) values where monitored. For EIS measurements 0.12 V (half-wave potential of the redox pair) was applied, in a frequency range from 10000 Hz to 0.1 Hz, amplitude 10 mV. The resistance to charge transfer (R_{CT}) values were calculated utilizing NOVA 2.1.3 software, fitting the experimental data of the Nyquist plots in the equivalent circuit, with a $\chi^2 < 10^{-2}$.

2.6 Morphological characterization of the electrodes

The surface morphology of the electrodes was assessed by scanning probe microscopy (Model 5100 N, Hitachi), performed in atomic force microscopy (AFM) mode, and by scanning electron microscopy (SEM) on an EVO MA10 Zeiss microscope. AFM microscopies were analyzed with Gwyddion 2.58 software.

2.7 Faradaic detections of complementary target and real samples

Square wave voltammetry (SWV) and faradaic EIS detections were performed onto the electrode to verify successful DNA hybridization, utilizing complementary and non-complementary oligonucleotide sequences as target. 10 µL of the target solution (10 µmol L^{-1}, PBS) was applied onto the SPCE working area and kept at 57 ºC (the annealing temperature of the probe DNA with the complementary target) for 20 min. The electrode was washed by immersion in PBS for 10 s and dried with N_2. The values of peak current (I_p) were monitored by SWV, applying a potential from -0.1 V to +0.4 V, amplitude 25 mV, increment 4 mV, frequency 15 Hz, in ferrocyanide/ferricyanide redox pair solution ($K_4[Fe(CN)_6]$ and $K_3[Fe(CN)_6]$, 1 mmol L^{-1}, in PBS 10 mmol L^{-1}. Faradaic EIS was carried out as described in item 2.5. The prepared pure beef and pork samples were also used

for faradaic detection to ensure that its components do not interfere with the DNA hybridization onto the biosensor surface.

2.8 Non-faradaic detections of real samples

For the construction of a calibration curve, the normalized meat samples were mixed in different proportions (v/v) as follows: 100% pork (total positive sample), 100% beef (total negative sample), a mixture of 50% each, 90% beef with 10% pork and 99% beef with 1% pork. 10 µL of the samples were applied onto the SPCE working area and kept at 57 ºC for 20 min. The electrode was washed by immersion in PBS for 10 s and dried with N_2. A blank sample (PBS only) was also used. Electrochemical detection of the target was performed by non-faradaic EIS (0 V, frequency range from 10000 Hz to 0.1 Hz, amplitude 10 mV) in PBS solution. The admittance and impedance values were calculated utilizing the NOVA 2.1.3 software, fitting the experimental data of the Nyquist and Bode plots in the equivalent circuit, with a $\chi^2 < 10^{-2}$.

2.9 Stability study

To determine the stability of the genosensor, the prepared bioelectrodes were maintained in a sealed container, with atmospheric air at room temperature for 4 weeks. Analysis by non-faradaic EIS using pure pork samples were conducted each week, in order to evaluate whether the biosensor was still functional and could recognize its target.

3 RESULTS AND DISCUSSION

3.1 Electrochemical characterizations

It was observed that from the initial 1.00 mg mL^{-1} of suspended graphene acid, an average of 0.45 mg mL^{-1} was obtained in the final supernatant after centrifugation. The sonication and centrifugation steps of the graphene acid suspension aim to discard large clumps of nanomaterial, in order to obtain the lightest and loosest sheets to enhance the drop-cast procedure. The repetition of

the drop-casting for two consecutive times showed the lowest resistance values and the highest current (Fig. S1), so it was maintained for further analysis. That can be explained because one drop-casting round is not enough to cover the entire working electrode surface with the nanomaterial, while in three repetitions or more there is an accumulation of nanomaterial, and its electronic properties diminished.

The electrochemical properties of the graphene acid-coated SPCE were probed with cyclic voltammetry in ferro/ferricyanide aqueous electrolyte (Fig. 3A, data in Table S1). For the case of the bare SPCE, the oxidation potential of ferrocyanide was the highest measured (0.301 ± 0.021 V), while the anodic peak current was the lowest (14.39 ± 1.56 µA). After the modification of SPCE with graphene acid, a decrease in the oxidation potential (0.176 ± 0.015 V) and an increase in anodic peak current (23.48 ± 2.24 µA) were recorded, indicating a more facile oxidation of ferrocyanide, and improved charge-transport properties, respectively. These data support the capability of graphene acid to promote the electrocatalytic redox reactions on the electrode, due to its higher conductivity, as shown by the 14 times higher charge transfer resistance of the bare SPCE (12.54 ± 1.19 kΩ, Fig. 3B) in comparison to the graphene acid modified one (0.85 ± 0.07 kΩ). The improved performance may also be affected by the higher surface area of the electrode after deposition of graphene acid (as later discussed).

<FIGURE 3>

The modification of the electrode with the DNA probe decreased the oxidation current (17.83 ± 1.64 µA) and shifted the potential to a slightly anodic value (0.204 ± 0.018 V) in comparison with the graphene acid-modified SPCE. This can be attribute to two main causes: 1) the inherent steric hindrance of the DNA molecules that prevents the ferro/ferricyanide ions from reaching the electrode surface, and 2) the negative net charge of the biomolecule, due to the presence of negatively charged phosphate groups in a neutral medium (PBS, pH = 7.4), thus also repelling the negatively charged ferro/ferricyanide ions. Likewise, the resistance to charge transfer

mean increased in 2 kΩ after the DNA probe incorporation, indicating that the biomolecule is well incorporated into the working electrode surface by the EDC/NHS mechanism which links the carboxyl groups of the nanomaterial to the amino group of the biomolecule. The FTIR analysis (Fig. S2) also indicates the bond formation between the DNA probe and the electrode surface with the EDC/NHS protocol, as there is an increase in the band region between 1510 to 1700 cm^{-1}, which involves the 1665 cm^{-1} characteristic amide I band, as well a small band in 1700 cm^{-1} corresponding to the amide carbonyl band. There was also an increase in the amide A band (around 3500 cm^{-1}), another characteristic band, showing the formation of the amide bond between the carboxylic group of GA and the amino group of the DNA 5' end, mediated by the EDC/NHS chemical mechanism.

3.2 Morphological characterizations

The analysis of the electrode morphology can provide interesting data in relation to the behavior of the nanomaterial on the solid surface and can also corroborate with the electrochemical analysis. Fig. 4 shows SEM and AFM images of the working electrode in the genosensor construction steps and Table S2 summarizes some surface parameters extracted from AFM microscopy. Printed carbon electrodes usually have rough texture due to ink constituents, as can be observed in the morphology in SEM images and the roughness coefficient of the bare SPCE (120.15 ± 9.78 nm, surface area of 33.19 ± 4.91 μm^2). The addition of GA promotes an increase in this inherent roughness (R_q = 209.84 ± 21.67 nm), in addition to an increase of more than three times in the surface area of the electrode (106.54 ± 11.45 μm^2). The surface area increase can be associated with the electrochemical results which showed an increase in the current and a decrease in the charge transfer resistance after graphene acid deposition. The incorporation of the DNA probe caused a small drop in the roughness and surface area values (183.67 ± 15.45 nm and 90.47 ± 10.56 μm^2, respectively), that can be attributed to the formation of cross-links between the nanomaterial and the biomolecule.

<FIGURE 4>

3.3 Faradaic detections of complementary target and meat samples

To ensure that the genosensor is working properly and the real sample is recognized by the immobilized DNA probe, complementary targets and pure pork and beef samples were detected by SWV (Fig. 3C) and by faradaic EIS (Fig. 3D). Without any target, the genosensor presented with the highest peak current and lowest resistance to charge transfer values (I_P = 12.63 ± 1.43 µA and R_{CT} = 2.91 ± 0.21 kΩ, Table S3), since electron transfer is less impeded in absence of the complementary target. Similar values were recorded in presence of non-complementary target (I_P = 11.35 ± 1.09 µA, R_{CT} = 3.14 ± 0.29 kΩ) and the beef sample (I_P = 11.07 ± 1.04 µA, R_{CT} = 3.75 ± 0.36 kΩ), highlighting the absence of any binding events on the graphene acid modified SPCE and the selectivity of the genosensor. On the other hand, the application of the complementary DNA solution decreased the Ip and raised the R_{CT} values (7.26 ± 0.85 µA, 6.23 ± 0.57 kΩ). Due to hybridization of the complementary DNA strands, the quantity of biomolecules on the surface increases and leads to greater steric hindrance, which obstructs the ferrocyanide ions from reaching the electrode surface. The presence of pork sample resulted in the lowest peak current and highest resistance to charge transfer values (6.89 ± 0.71 µA, 7.64 ± 0.71 kΩ), because it is a more complex sample and contains larger fragments of mitochondrial DNA, thus creating a greater electron transfer barrier during the redox events. The DNA probe sequence was selected to be complementary to the pork cytochrome b gene because that is a barcode gene, as it is used to discern different species as it is highly specific. In addition, the use of a mitochondrial DNA sequence has the advantage that this genetic material is present in greater amounts in muscle tissue than nuclear DNA, facilitating its detection.

3.4 Non-faradaic detection of the meat samples

Pure pork and beef samples were analyzed by non-faradaic EIS, and the Nyquist and Bode plots where extracted (Fig. 5A and 5B, respectively). Non-faradaic impedance was employed because it is the only operative electrochemical technique in the absence of any redox label in the electrolyte solution. Thus, the charge transfer-related parameters (R_{CT} and Warburg diffusional impedance) are negligible, and the equivalent Randles circuit can be simulated only by considering the solution resistance (R_S) and a capacitor element. Due to the use of an imperfect rough carbon electrode, the capacitor element is substituted for a constant phase element (CPE). In this case, the Nyquist plot assumes a straight-line (Fig. 5A) that forms an angle to the real impedance axis. This angle is proportional to how similar the CPE is in relation to a real capacitor, as a perfect capacitor assumes a vertical straight-line in the Nyquist Plot. The Impedance Bode plot (Fig. 5B, black lines) forms two regions: a horizontal region at high frequencies, corresponding to the resistance of the electrolytic solution, and a sloped region at low frequencies, corresponding to the CPE. In the Bode plot from Figure 5B, at frequencies of 10 Hz and below, the impedance response is driven by the capacitive reactance, indicating the non-faradaic charging of the double layer (Stevenson et al., 2018).

<FIGURE 5>

The CPE admittance values (Y_0) can be obtained by fitting the experimental data with a simple equivalent circuit. Admittance can be defined as how easily a circuit or device will allow a current to flow, and it varies according to the electrode surface coverage (Lee and Shim, 2001). In a non-faradaic experiment, the presence of biomolecules on the electrode surface will disturb the delicate electrical double layer formation due to electrostatic interactions with the electrolyte solution ions. Therefore, the higher the concentration of biomolecules on the electrode surface, the lower the admittance values of the formed double electric layer against the sinusoidal perturbation. Considering the greater retention of pork DNA on the electrode surface, due to its hybridization

with the immobilized probe, a major disruption in the double electrical layer is observed, as indicated by a decrease of 22% in its CPE admittance values (38.23 ± 0.76 µS s^N in pork versus 49.44 ± 0.98µS s^N in beef).

The impedance values also demonstrated differences between the samples: in low frequency regions (starting in 10 Hz, constant after that) there was an 20% increase in the total impedance values (Z) with the addition of the pork sample (50.76 ± 1.54 kΩ in f = 1 Hz) in comparison to the beef sample (40.69 ± 0.85 kΩ in f = 1 Hz). This observation corroborates with the decrease in the admittance because they are inverse parameters: the presence of more biomolecules on the electrode surface results in a greater steric hindrance, leading to a greater impedance at lower frequencies to the sinusoidal disturbance.

3.5 Calibration curves and genosensor stability

Two calibration curves were constructed, based on the admittance values (Fig. 5C) and on the total impedance values at low frequency (Fig. 5D). A linear behavior was observed for both variables, and the experimental calibration curves were fitted by linear equations: Y_0 = 49.123 - 0.109*(pork content percentage), r = 0.997 (n = 3) and Z = 40.95 + 0.096*(pork content percentage), r = 0.991 (n = 3). We verified that the admittance was a more adequate parameter for measurement, since it presented a slightly higher slope value, which indicates a greater sensitivity, and a higher r coefficient, implying better linearity, both desired analytical parameters for biosensors. The calculated limit of detection (LOD = 3*blank standard deviation/slope) was 9.35% of pork content in beef. As this LOD was obtained with a non-purified and non-amplified sample, it is possible that trace levels detection could be achieved with sample purification and amplification steps.

The stability study (Fig. 5E) showed that the biosensor remained functional even after 4 weeks of storage at room temperature, as the electrochemical parameters of the detection of pork

residues in beef remained practically intact: after 28 days the signals varied by 3.2% for admittance and 3.6% for impedance.

Biosensors based in nucleic acids for pork detection in meat samples are scarce in the literature (Table 1). Most reported genosensors require long sample preparation and assay time, while platform stability studies of such sensors remained vastly unexplored, although it is an important parameter for defining the shelf-life of the biosensor, dictating its future potential for commercialization. Although this work reports a higher detection limit than some previously developed biosensors, it is necessary to emphasize that it did not require any DNA purification or amplification technique, nor was any electrochemical indicator or redox molecule required for detection, and it presented a simple drop-casting protocol for electrode surface modification. These features render the present pork-residue detecting genosensor as the most sensitive one among the label-free and reagentless sensors in the field.

4 CONCLUSIONS

The combination of a cost effective lab-made screen-printed carbon electrode, with a selective and densely functionalized graphene derivative with carboxyl groups, and further modified with a single stranded DNA probe, resulted in an impedimetric diagnostic device that can detect adulteration of beef by pork with a limit of detection of 9% w/w. Importantly, the overall protocol and the impedimetric technique are simple, without requiring expensive and/or hazardous reagents, neither extensive purification steps or amplification of the target genetic material in the sample. Furthermore, the method has a sample preparation and assay time of 45 minutes, and the sensor retains its full functional performance for at least 4 weeks of storage.

These set of features places the present pork DNA sensor among the most attractive for further development and commercialization. Electrochemical biosensors that use non-faradic techniques are scarce in the scientific literature, especially employing DNA as a biorecognition element. Therefore, this work lays the ground for the development of new biosensing devices that

do not require specific reagents for detection and that are truly label-free, powered by the recent achievements in fluorographene's chemistry. In addition, the reported platform has the potential for immobilization of other DNA sequences specific to a multitude of targets, thus tremendously expanding its application potential in the biomedical, crop and food analysis fields.

Acknowledgments

We acknowledge the financial support from the EU Graphene Flagship Core 2 Project (No. 785219). This article reflects only the author's view, and the European Commission is not responsible for any use that may be made of the information it contains. ICN2 is funded by the CERCA programme, Generalitat de Catalunya. The ICN2 is supported by the Severo Ochoa Centres of Excellence programme, funded by the Spanish Research Agency (AEI, grant no. SEV-2017-0706). J. M. R. Flauzino is grateful for the Coordenação de Aperfeiçoamento de Pessoal de Nível Superior scholarship (CAPES-PRINT, Brazil, Grant number: 88887.371591/2019-00). D. Panáček acknowledges the Internal Student Grant Agency of the Palacký University in Olomouc, (IGA_PrF_2021_031). A. G. Brito-Madurro acknowledges the funding from Conselho Nacional de Desenvolvimento Científico e Tecnológico - CNPq (310782/2018-0). J. M. Madurro acknowledges the funding from Fundação de Amparo à Pesquisa do Estado de Minas Gerais – FAPEMIG (CEX-APQ-02902-17) and Conselho Nacional de Desenvolvimento Científico e Tecnológico – CNPq (311737/2018-8). A. Bakandritsos acknowledges the funding from the Czech Science Foundation, (project GA CR – EXPRO, 19-27454X). M. Otyepka acknowledges the ERC grand 2D-CHEM (No 683024 from H202). The work was supported also by the ERDF/ESF project "Nano4Future" (No.CZ.02.1.01/0.0/0.0/16_019/0000754).

References

Ahmed, M.U., Hasan, Q., Mosharraf, M.H., Saito, M., Tamiya, E., 2010. Food Control 21, 599–605.

Ali, M.E., Hashim, U., Mustafa, S., Che Man, Y.B., Yusop, M.H.M., Kashif, M., Dhahi, T.S., Bari, M.F., Hakim, M.A., Latif, M.A., 2011. J. Nanomater. 2011, 1–11.

Ali, M.E., Hashim, U., Mustafa, S., Che Man, Y.B., Islam, K.N., 2012. J. Nanomater. 2012.

Alves-Balvedi, R.P.P., Caetano, L.P.P., Madurro, J.M.M., Brito-Madurro, A.G.G., 2016. Biosens. Bioelectron. 85, 226–231.

Bakandritsos, A., Pykal, M., Błoński, P., Jakubec, P., Chronopoulos, D.D., Poláková, K., Georgakilas, V., Čépe, K., Tomanec, O., Ranc, V., Bourlinos, A.B., Zbořil, R., Otyepka, M., 2017. ACS Nano 11, 2982–2991.

Berggren, C., Stålhandske, P., Brundell, J., Johansson, G., 1999. Electroanalysis 11, 156–160.

Blanco, M., Mosconi, D., Otyepka, M., Medveď, M., Bakandritsos, A., Agnoli, S., Granozzi, G., 2019. Chem. Sci. 10, 9438–9445.

Cecchetto, J., Fernandes, F.C.B., Lopes, R., Bueno, P.R., 2017. Biosens. Bioelectron. 87, 949-956.

Chen, H.J., Chen, R.L.C., Hsieh, B.C., Hsiao, H.Y., Kung, Y., Hou, Y. Te, Cheng, T.J., 2019. Biosens. Bioelectron. 131, 53–59.

Chronopoulos, D.D., Bakandritsos, A., Pykal, M., Zbořil, R., Otyepka, M., 2017. Appl. Mater. Today. 9, 60–70.

De Castro, A.C.H., Kochi, L.T., Moço, A.C.R., Coimbra, R.S., Oliveira, G.C., Cuadros-Orellana, S., Madurro, J.M., Brito-Madurro, A.G., 2018. J. Solid State Electrochem. 22, 2339–2346.

De La Escosura-Muñiz, A., Baptista-Pires, L., Serrano, L., Altet, L., Francino, O., Sánchez, A., Merkoçi, A., 2016. Small 12, 205–213.

El Sheikha, A.F., 2019 Trends Food. Sci. Technol. 86, 544–552.

Flauzino, J.M.R., Peres, R.C.S., Alves, L.M., Vieira, J.G., dos Santos, J.G., Brito-Madurro, A.G.,

Madurro, J.M., 2021a. Bioelectrochemistry 140, 107801.

Flauzino, J.M.R., Pimentel, E.L., Alves, L.M., Madurro, J.M., Brito-Madurro, A.G., 2021b. Electroanalysis 33, 296-303.

Hansen, A., 2018. Geoforum 93, 57–68.

Hellberg, R.S., Hernandez, B.C., Hernandez, E.L., 2017. Food Control 80, 23–28.

Heng Cheong, Y., Nasir, M.Z.M., Bakandritsos, A., Pykal, M., Jakubec, P., Zbořil, R., Otyepka, M., Pumera, M., 2019. ChemElectroChem 6, 229–234.

Idili, A., Parolo, C., Alvarez-Diduk, R., Merkoçi, A., 2021. ACS Sensors

Irwin, D.M., Kocher, T.D., Wilson, A.C., 1991. J. Mol. Evol. 32, 128–144.

Khairil Mokhtar, N.F., El Sheikha, A.F., Azmi, N.I., Mustafa, S., 2020. J. Sci. Food Agric. 100, 1687–1693.

Kumar, Y., Bansal, S., Jaiswal, P., 2017. Compr. Rev. Food Sci. Food Saf. 16, 1359–1378.

Lee, T.Y., Shim, Y.B., 2001. Anal. Chem. 73, 5629–5632

Lenarda, A., Bakandritsos, A., Bevilacqua, M., Tavagnacco, C., Melchionna, M., Naldoni, A., Steklý, T., Otyepka, M., Zbořil, R., Fornasiero, P., 2019. ACS Omega 4, 19944–19952.

Matsunaga, T., Chikuni, K., Tanabe, R., Muroya, S., Shibata, K., Yamada, J., Shinmura, Y., 1999.. Meat Sci. 51, 143–148.

Merkoçi, A., 2010. Biosens. Bioelectron. 26 (4), 1164-1177

Moço, A.C.R., Guedes, P.H., Flauzino, J.M.R., da Silva, H.S., Vieira, J.G., Castro, A.C.H., Gomes, É.V.R., Tolentino, F.M., Soares, M.M.C.N., Madurro, J.M., Brito-Madurro, A.G., 2019. Electroanalysis 31, 1580–1587.

Montiel, V.R.V., Gutiérrez, M.L., Torrente-Rodríguez, R.M., Povedano, E., Vargas, E., Reviejo, Á.J., Linacero, R., Gallego, F.J., Campuzano, S., Pingarrón, J.M., 2017. Anal. Chem. 89, 9474–9482.

Okuma, T.A., Hellberg, R.S., 2015. Food Control 50, 9–17.

Oliveira, D.A., de Rezende Rodovalho, V., Flauzino, J.M.R., da Silva, H.S., Araujo, G.R., Vaz,

E.R., Vieira, C.U., Madurro, J.M., Madurro, A.G.B., 2018a. Protein Pept. Lett. 25, 878–883.
Oliveira, D.A., Silva, J. V., Flauzino, J.M.R., Castro, A.C.H., Moço, A.C.R., Soares, M.M.C.N., Madurro, J.M., Brito-Madurro, A.G., 2018b. Anal. Biochem. 549, 157–163.
Quesada-González, D., Merkoçi, A., 2018. Chem. Soc. Ver. 47, 4697–4709.
Rabti, A., Raouafi, N., Merkoçi, A., 2016. Carbon 108, 481–514.
Rahmati, S., Julkapli, N.M., Yehye, W.A., Basirun, W.J., 2016. Food Control 68, 379–390.
Ratajczak, K., Krazinski, B.E., Kowalczyk, A.E., Dworakowska, B., Jakiela, S., Stobiecka, M., 2018a. ACS Appl. Mater. Interfaces 10, 17028–17039.
Ratajczak, K., Krazinski, B.E., Kowalczyk, A.E., Dworakowska, B., Jakiela, S., Stobiecka, M., 2018b. Nanomaterials 8, 510.
Ribeiro, S.H.D., Alves, L.M., Flauzino, J.M.R., Moço, A.C.R., Segatto, M.S., Silva, J.P., Borges, L.F.A., Madurro, J.M., Madurro, A.G.B., 2020. Electroanalysis 32 (10), 2316-2322
Rosati, G., Ravarotto, M., Sanavia, M., Scaramuzza, M., De Toni, A., Paccagnella, A., 2019. Sens Bio-Sensing Res. 26, 100308.
Šedajová, V., Jakubec, P., Bakandritsos, A., Ranc, V., Otyepka, M., 2020. Nanomaterials 10, 1–14.
Seelajaroen, H., Bakandritsos, A., Otyepka, M., Zbořil, R., Sariciftci, N.S., 2020. ACS Appl. Mater. Interfaces 12, 250–259.
Singh, P.K., Jairath, G., Ahlawat, S.S., Pathera, A., Singh, P., 2016. J. Food Sci. Technol. 53, 1759–1765.
Stevenson, H., Radha Shanmugam, N., Paneer Selvam, A., Prasad, S., 2018. SLAS Technol. 23, 5–15.
Strong, M.E., Richards, J.R., Torres, M., Beck, C.M., La Belle, J.T., 2021. Biosens. Bioelectron. 177, 112949.
Thiyagarajan, N., Chang, J.L., Senthilkumar, K., Zen, J.M., 2014. Electrochem. Commun. 38, 86–90.
Torelli, E., Manzano, M., Marks, R.S., 2017. Sens. Actuators B Chem. 247, 868–874.

Vermisoglou, E., Panáček, D., Jayaramulu, K., Pykal, M., Frébort, I., Kolář, M., Hajdúch, M., Zbořil, R., Otyepka, M., 2020. Biosens. Bioelectron. 166.

Wilson, J.M., Platts-Mills, T.A.E., 2018. Mol. Immunol. 100, 107–112.

FIGURES

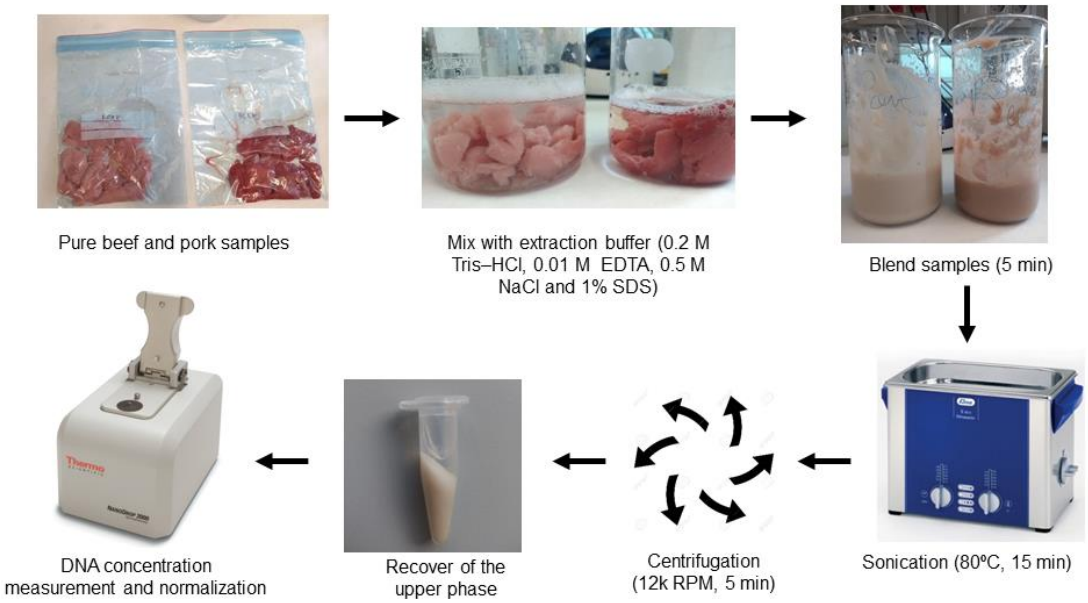

Figure 1 – Scheme of the meat sample preparation steps.

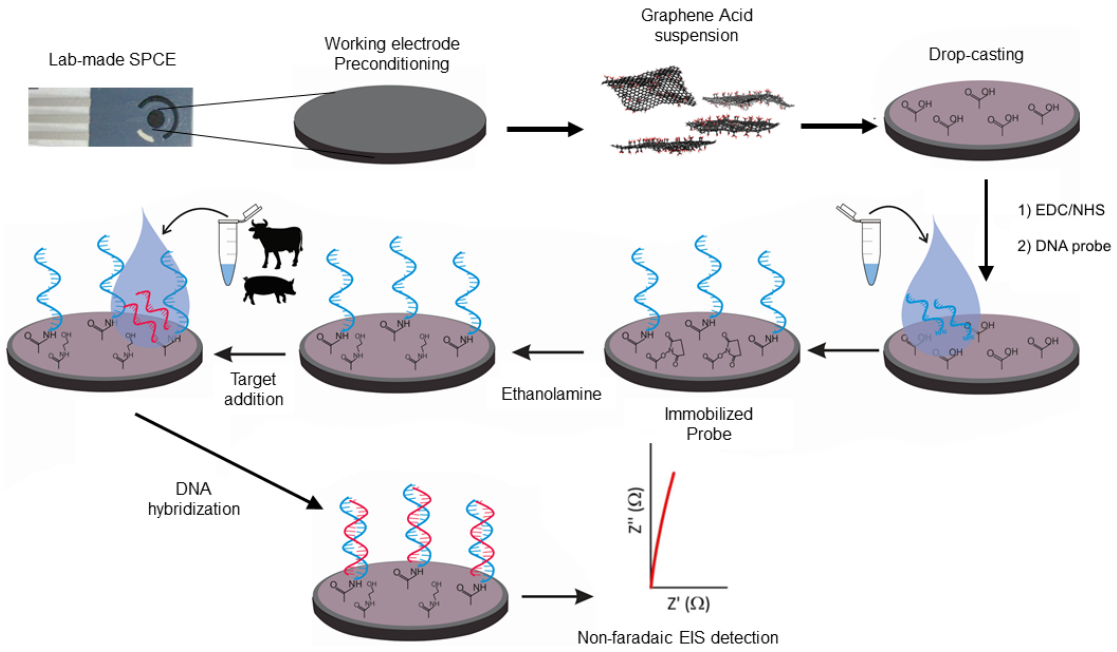

Figure 2 – Scheme of the SPCE modification and genosensor construction.

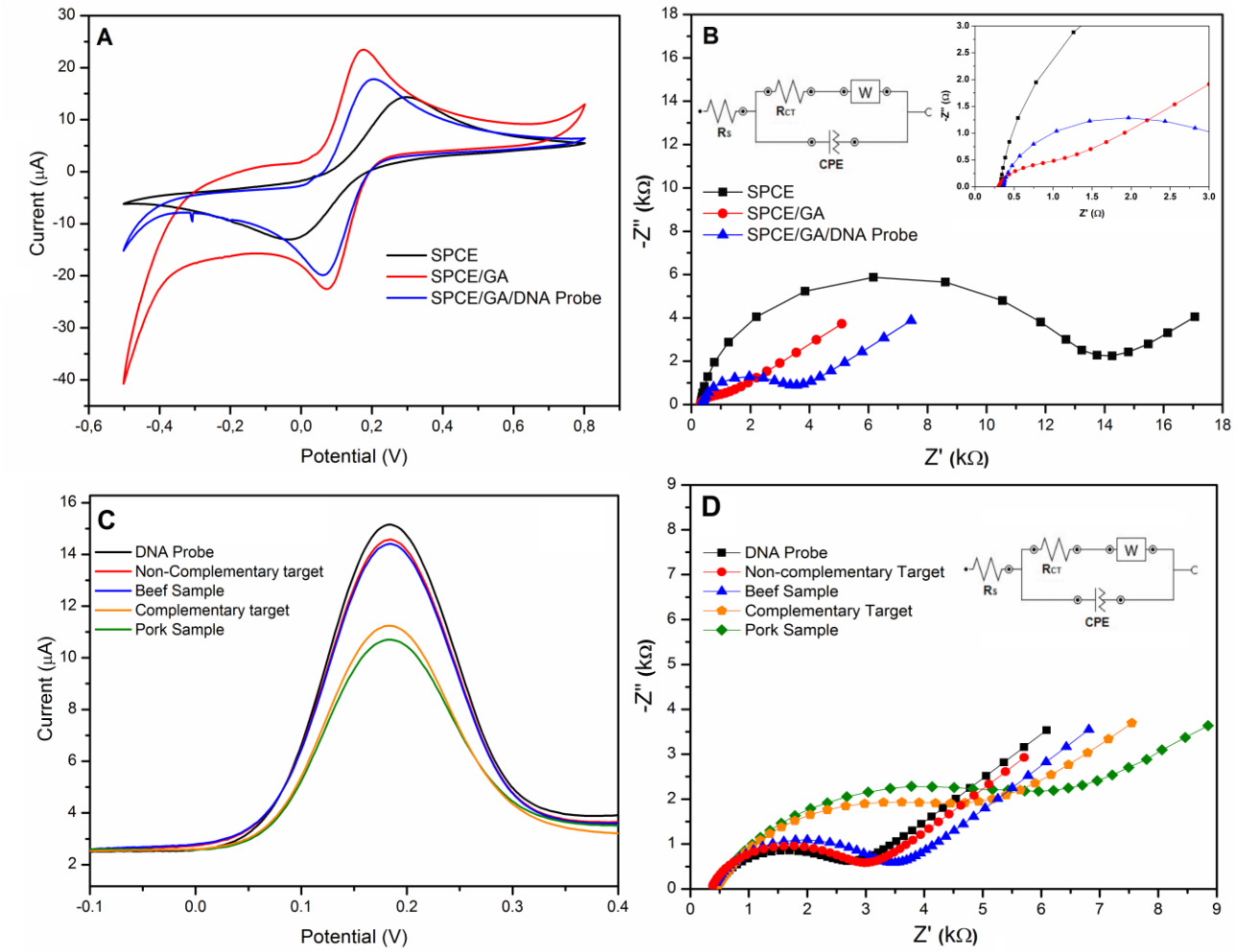

Figure 3 – Electrochemical characterization of the genosensor construction steps: **(A)** cyclic voltammograms of the bare screen-printed carbon electrode (SPCE), SPCE modified with graphene acid (SPCE/GA) and SPCE/GA after the immobilization of the DNA probe (SPCE/GA/DNA Probe). **(B)** Nyquist plots obtained by EIS analysis in each genosensor construction step; inset 1: equivalent Randles circuit, where R_S, R_{CT}, W, and CPE represent the solution resistance, the charge-transfer resistance, the Warburg diffusion resistance, and the constant phase element, respectively; inset 2: high-frequency region zoom. Faradaic detections of complementary target and meat samples: **(C)** square wave voltammograms and **(D)** Nyquist plots obtained by EIS; inset: equivalent Randles circuit. Electrolyte: PBS (10 mmol L^{-1}), containing $K_4[Fe(CN)_6]$ and $K_3[Fe(CN)_6]$ (1 mmol L^{-1}). CV parameters: potential range from -0.5 to 0.8 V, 50 mV s^{-1}. EIS parameters: frequency range from 10000 Hz to 0.1 Hz, potential applied 0.12V, amplitude 10 mV.

SWV parameters: potential range from -0.1 V to +0.4 V, amplitude 25 mV, increment 4 mV, frequency 15 Hz.

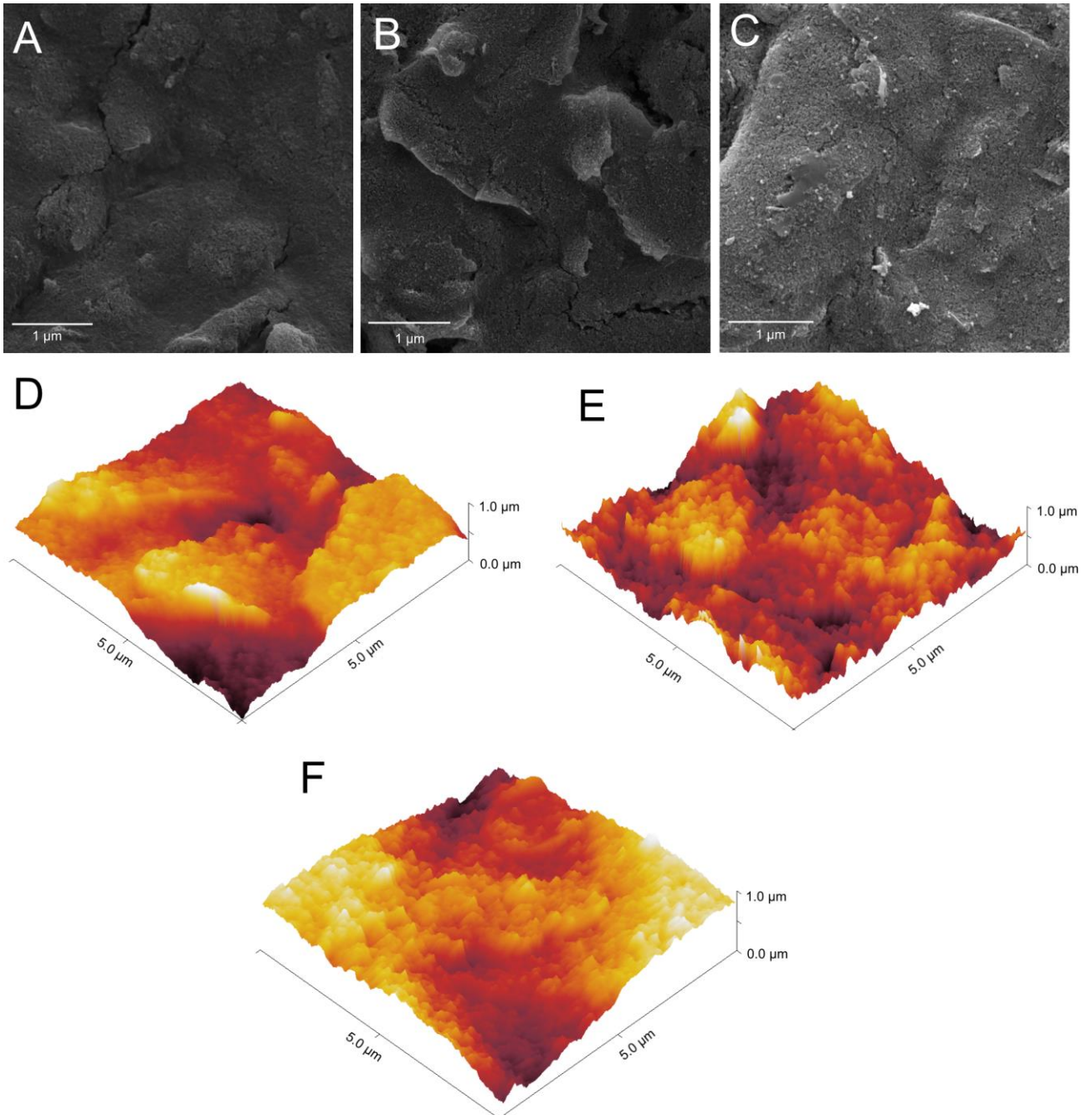

Figure 4 – Scanning Electron and Atomic Force micrographs of the working electrode of the bare SPCE **(A, D)**, SPCE modified with graphene acid **(B, E)** and SPCE modified with graphene acid and the DNA probe **(C, F)**.

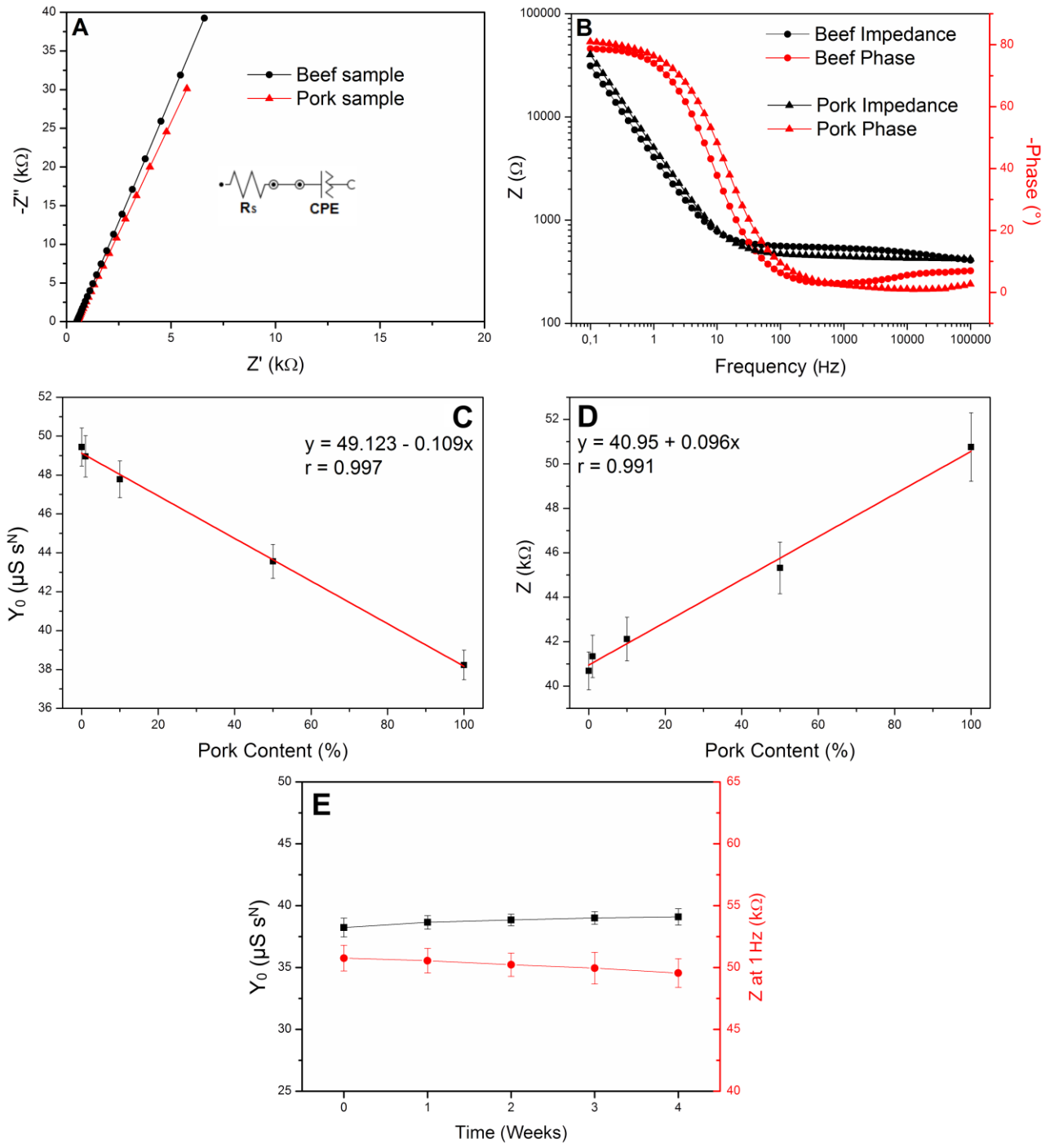

Figure 5 – Detection of pork and beef samples with non-faradaic electrochemical impedance spectroscopy: **(A)** Nyquist plots. Inset: equivalent Randles circuit where R_S is the electrolyte solution resistance and CPE is the constant phase element. **(B)** Bode plots with total impedance (Z) and Phase values in function of the frequency. Calibration curves of the developed biosensor based on **(C)** admittance values and **(D)** total impedance values (f = 1 Hz). (**E**) Stability of the genosensor response over time with a pure pork sample in function of time. Electrolyte: PBS (10 mmol L^{-1}), frequency range from 10000 Hz to 0.1 Hz, potential applied 0 V, amplitude 10 mV. Data is presented as mean ± standard deviation, n = 3.

Table 1 – Reported genosensors for detection of pork DNA in beef samples.

Platform	Detection method/technique	Label-free and Reagentless	Detection limit	DNA purification and/or amplification	Sample preparation and assay time	Stability	Ref
Optical fiber	Chemiluminescent	No	1% w/w	Yes	150 min	n. a.	(Torelli et al., 2017)
Gold Nanoparticles	Spectrophotometry	Yes	10% w/w	Yes	n. a.	n. a.	(Ali et al., 2012)
Lateral Flow	Naked eye	No	0.1% w/w	No	45 min	n. a.	(El Sheikha, 2019)
Disposable electrochemical printed chips	Linear Sweep Voltammetry	No	20% w/w	Yes	65 min	n. a.	(Ahmed et al., 2010)
Gold Nanoparticles	Spectrophotometry	No	1% w/w	Yes	150 min	n. a.	(Ali et al., 2011)
Graphite disk modified with polymeric nanocomposite	SWV and Faradaic EIS	No	1% w/w	No	60 min	4 weeks	(Flauzino et al., 2021b)
SPCE modified with Graphene Acid	Non-faradaic EIS	Yes	9% w/w	No	45 min	4 weeks	This work

n. a.: not available

LABEL-FREE AND REAGENTLESS ELECTROCHEMICAL GENOSENSOR BASED ON GRAPHENE ACID FOR MEAT ADULTERATION DETECTION

José M. R. Flauzino, Emily P. Nguyen, Qiuyue Yang, Giulio Rosati, David Panáček, Ana G. Brito-Madurro, João M. Madurro, Aristeidis Bakandritsos, Michal Otyepka, Arben Merkoçi

Supplementary Material

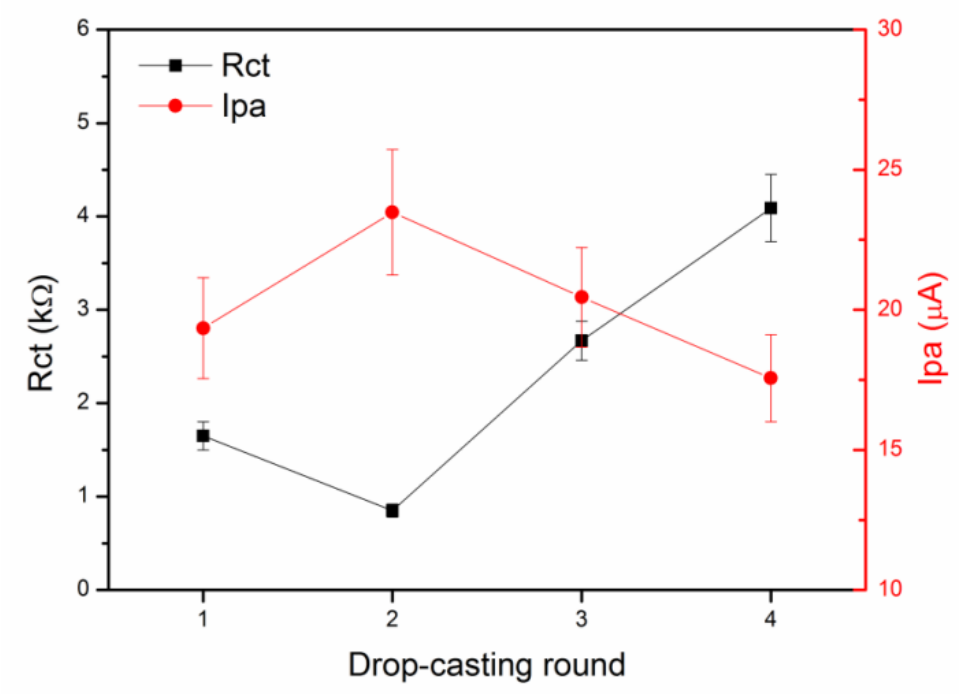

Figure S1 – Optimization of the drop-casting procedure of the graphene acid solution: electrochemical characterization of the electrode surface. Electrolyte: PBS (10 mmol L^{-1}), containing $K_4[Fe(CN)_6]$ and $K_3[Fe(CN)_6]$ (1 mmol L^{-1}). CV parameters: potential range from -0.5 to 0.8 V, 50 mV s^{-1}. EIS parameters: frequency range from 10000 Hz to 0.1 Hz, potential applied 0.12V, amplitude 10 mV.

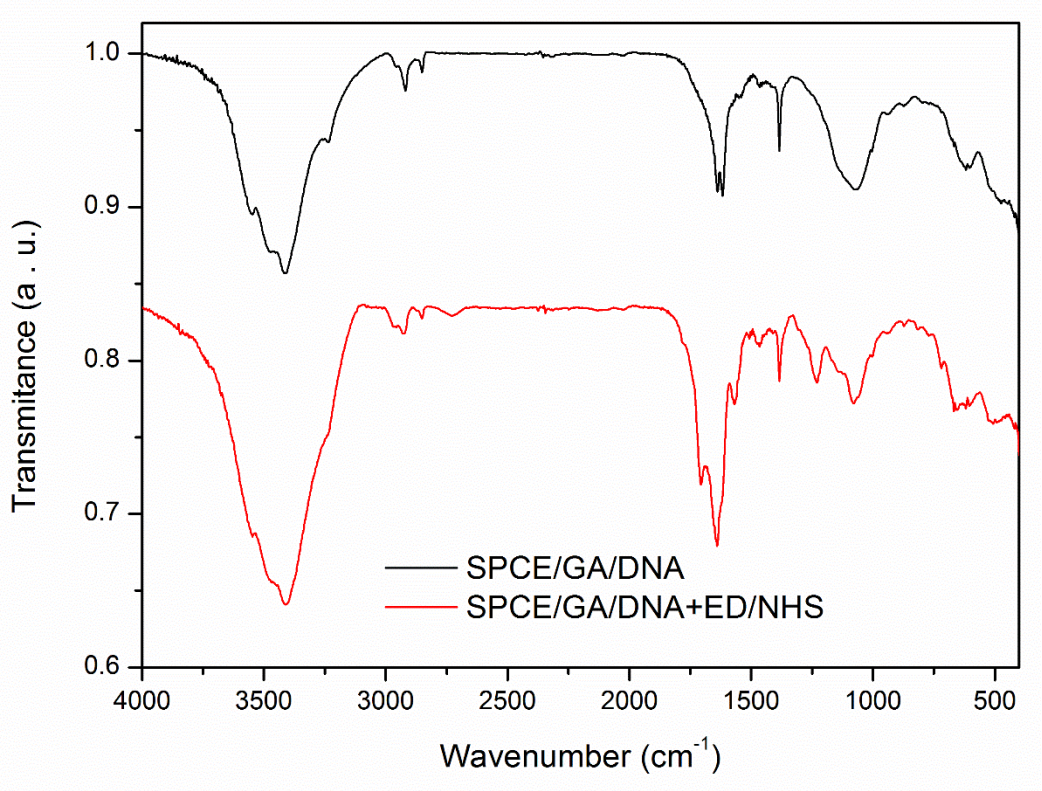

Figure S2 – FTIR spectra of the SPCE with and without the application of the linker EDC/NHS.

Table S1 – Electrochemical data of the biosensor characterization steps (mean ± standard deviation, n=3)

Electrode	**i_{pa} (µA)**	**E_{pa} (V)**	**R_{CT} (kΩ)**
SPCE	14.39 ± 1.56	0.301 ± 0.021	12.54 ± 1.19
SPCE/GA	23.48 ± 2.24	0.176 ± 0.015	0.85 ± 0.07
SPCE/GA/DNA probe	17.83 ± 1.64	0.204 ± 0.018	2.91 ± 0.217

Table S2 – Surface parameters extracted from AFM microscopies.

Electrode Surface	**Root Mean Square Roughness (nm)**	**Surface Area (µm²)**
SPCE	120.15 ± 9.78	33.19 ± 4.91
SPCE/GA	209.84 ± 21.67	106.54 ± 11.45
SPCE/GA/DNA	183.67 ± 15.45	90.47 ± 10.56

Table S3 – Electrochemical data of faradaic detections of targets (mean ± standard deviation, n = 3)

Target sample	**i_p (µA)**	**R_{CT} (kΩ)**
None (probe only)	12.63 ± 1.43	2.91 ± 0.21
Non-Complementary target	11.35 ± 1.09	3.14 ± 0.29
Complementary target	7.26 ± 0.85	6.23 ± 0.57
Pure Beef	11.07 ± 1.04	3.75 ± 0.36
Pure Pork	6.89 ± 0.71	7.64 ± 0.71

Table S4 - Electrochemical data obtained from non-faradaic EIS detections (mean ± standard deviation, n = 3)

Beef:Pork sample ratio (v/v)	**Y_0 (µS s^N)**	**Z at 1 hz (kΩ)**
100:0 (Pure beef)	49.44 ± 0.98	40.69 ± 0.85
99:1	48.96 ± 1.06	41,34 ± 0.95
90:10	47.78 ± 0.95	42.12 ± 0.98
50:50	43.56 ± 0.87	45.32 ± 1.16
0:100 (Pure Pork)	38.23 ± 0.76	50.76 ± 1.54
Blank (PBS)	52.68 ± 0.34	38.78 ± 0.76